Attitude Dynamics/Control of Dual-Body Spacecraft with Variable-Speed Control Moment Gyros

Marcello Romano and Brij N. Agrawal

Naval Postgraduate School, Monterey, California 93943

The dynamics equations of a spacecraft consisting of two bodies mutually rotating around a common gimbal axis are derived by the use of the Newton–Euler approach. One of the bodies contains a cluster of single-gimbal variable-speed control moment gyros. The equations include all of the inertia terms and are written in a general form, valid for any cluster configurations and any number of actuators in the cluster. A guidance algorithm has been developed under the assumtion that the two bodies of the spacecraft are optically coupled telescopes that relay laser signals. The reference maneuver is found by the imposition of the connectivity between the source and the target on the ground. A new nonlinear control law is designed for the spacecraft attitude and joint rotation by the use of Lyapunov's direct method. An acceleration-based steering law is used for the variable-speed control moment gyros. The analytical results are tested by numerical simulations conducted for both regulation and tracking cases.

I. Introduction

THE dynamics and control of multibody spacecraft are a challenging problem because of the complexity of the dynamics equations and the time-varying inertia of the system. The problem becomes even more interesting when gimbaled momentum exchange devices are considered to control attitude.

Control moment gyros (CMGs) are unique among attitude control actuators because they can provide high output torque without using expendable fuels and can provide a level of precision and continuity unachievable with jet thrusters. Indeed, CMGs have been used for decades on space stations and on military spacecraft when fast slewing capability and high pointing accuracy were required. The use of CMGs is also currently under consideration for several future civil spacecraft requiring high agility (as in Refs. 1 and 2).

A main drawback to the use of CMGs is the presence of singular gimbal-angle configurations at which the CMG cluster is unable to produce the required torque, or, in some cases, any torque at all.[3-5]

Many previous studies have considered the problem of the dynamics and control of spacecraft by the use of single-gimbal CMGs.

In particular, Oh and Vadali[6] report the complete equation of motions for the case of a single-body spacecraft and also consider the CMG's transverse and gimbal inertia; moreover, they introduce a nonlinear feedback control law and a singularity robust steering law. Schaub et al.[7] and Ford and Hall[8] propose the use of variable-speed CMGs (VS-CMGs), which add extra degrees of control to the classical CMG devices and may overcome the gimbal-angle singularities while maintaining the output torque equal to the requested one. Yoon and Tsiotras[9] consider the use of VS-CMGs for an integrated power/attitude control system.

In the present paper, the use of VS-CMGs is analyzed for a spacecraft consisting of two rigid bodies that can mutually rotate around a common gimbal axis. This high-level model represents the bifocal relay mirror spacecraft, which is under investigation at the Naval Postgraduate School and other institutions. The main mission of the bifocal relay mirror spacecraft, which consists of two mechanically and optically coupled telescopes, is to redirect a laser signal from ground-based sources to distant points on the Earth or in space. The receiver telescope captures the incoming energy from the laser

Marcello Romano is currently National Research Council Fellow and Associate Director of the Optical Relay Spacecraft Laboratory. He received his Ph.D. in aerospace engineering in 2001 and his Laurea degree (M.S.) in aerospace engineering in 1997, both from Politecnico di Milano, Italy. His main research interests are the dynamics and control of spacecrafts and space robots. Beyond analytical–numerical researches, he has been conducting extensive experimental activities with a number of advanced test-beds, both on the ground and in parabolic flights. For more information please see http://www.aa.nps.navy.mil/~mromano. Member AIAA.

Brij N. Agrawal is Distinguished Professor and Director of both the Spacecraft Research and Design Center and the Optical Relay Spacecraft Laboratory. He came to the Naval Postgraduate School in 1989 and since then has initiated a new M.S. curriculum in astronautical engineering in addition to establishing the Spacecraft Research and Design Center. He has developed research programs in attitude control of flexible spacecraft, smart structures, and space robotics. He received his Ph.D. in mechanical engineering from Syracuse University in 1970 and his M.S. in mechanical engineering from McMaster University in 1968. Associate Fellow AIAA.

source, whereas the transmitter telescope directs the laser beam at the target.

Previous analytical–numerical studies on the bifocal relay mirror project have been conducted with the objective of performing preliminary simulations of the dynamics and control of the overall spacecraft with reaction wheels (RWs)[10] and the inclusion of a model of the optical subsystem.[11] A parallel research effort in progress intends to validate the analytical–numerical results through experiments on the ground.[12,13]

The main contributions of the research presented in this paper are as follows:

1) A dynamic model is provided that takes into account all of the inertia terms for a dual-body spacecraft with a generic number of single-gimbal VS-CMGs in a generic cluster configuration. The equations of motion are factorized in a way that facilitates the design of the control law.

2) A guidance algorithm is used to compute the reference spacecraft attitude and joint motion by geometric imposition of the relaying of optical signals through the spacecraft between two distant points on Earth.

3) A new, nonlinear feedback control law is designed and tested by numerical simulations for both tracking and regulation cases.

Section II of the paper presents the analytical model and develops the system's equations of motion. Section III outlines the guidance algorithm. Section IV introduces the control laws. Finally, the simulation results are reported in Sec. V.

II. Analytical Model of the System Dynamics

In this section, we derive the equations of motion, with the Euler–Newton method, for a dual-body spacecraft containing a cluster of VS-CMGs. The approach is based on the work in Refs. 6–8 and 14 for the theory of vectrices. (A vectrix associated to a reference frame is defined in Ref. 14 as a column matrix, whose elements are a set of basis vectors for that frame.)

A. Rigid Body with One VS-CMG

Let us consider first a system of a rigid-body spacecraft B and one single-gimbal VS-CMG W, as in Fig. 1a. The system is free to move with respect to an inertial frame with vectrix $\mathbb{F}_i$.

A frame with vectrix $\mathbb{F}_b$ is fixed with the spacecraft body, and a frame with vectrix $\mathbb{F}_g \triangleq [\underline{a}_s \ \underline{a}_g \ \underline{a}_t]^T$ is fixed with the gimbal of the VS-CMG. Here, $\underline{a}_s$ is the unit vector directed as the rotor spin axis, $\underline{a}_g$ is directed as the gimbal rotation axis, and $\underline{a}_t = \underline{a}_s \times \underline{a}_g$ is directed as the torque produced by the VS-CMG.

First, the vectorial equations of rotational motion are found. The angular momentum of the overall system with respect to its center of mass O is given by the sum of the absolute angular momentum $\underline{h}_b$ of the spacecraft body with respect to O, the absolute angular momentum $\underline{h}_w$ of the VS-CMG with respect to its center of mass O_w, and the term of parallel transport from O_w to O

$$\underline{h}_O = \underline{h}_b + \underline{h}_w + m_w \left(r_w^2 \underline{1} - \underline{r}_w \underline{r}_w \right) \cdot \underline{\omega} \qquad (1)$$

where $\underline{h}_b = \underline{J}_b \cdot \underline{\omega}$ and $\underline{1}$ is the unit dyadic. The term $\underline{\omega}$ is the angular velocity of the rigid-body frame with respect to the inertial frame, $\underline{J}_b$ is the dyadic of inertia of the body with respect to O and $\underline{r}_w = O_w - O$. Absolute angular momentum $\underline{h}_w$ can be expressed as the sum of the contributions of the gimbal and the rotor

$$\underline{h}_w = \underline{h}_r + \underline{h}_g \qquad (2)$$

where $\underline{h}_r = \underline{J}_r \cdot \underline{\omega}_r$ and $\underline{h}_g = \underline{J}_g \cdot \underline{\omega}_g$. The terms $\underline{\omega}_r$ and $\underline{\omega}_g$ are, respectively, the absolute angular velocity of the VS-CMG rotor and gimbal, and $\underline{J}_r$ and $\underline{J}_g$ are the inertia dyadics. Introduction of the relative angular velocities of the gimbal with respect to the body, $\underline{\omega}_{gb}$, and of the rotor with respect to the gimbal, $\underline{\omega}_{rg}$, yields

$$\underline{h}_r = \underline{J}_r \cdot (\underline{\omega} + \underline{\omega}_{gb} + \underline{\omega}_{rg}), \qquad \underline{h}_g = \underline{J}_g \cdot (\underline{\omega} + \underline{\omega}_{gb}) \qquad (3)$$

The center of mass of the gimbal and rotor is assumed to coincide with the center of mass of the overall VS-CMG; as a consequence,
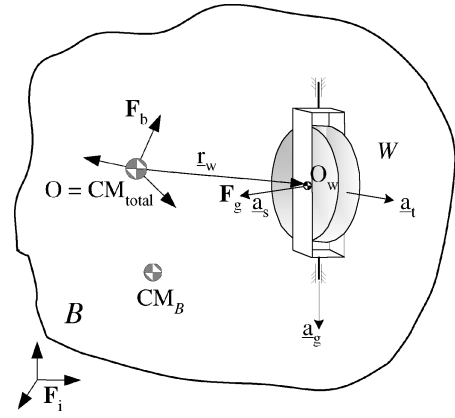
a) Spacecraft with a single-gimbal VS-CMG
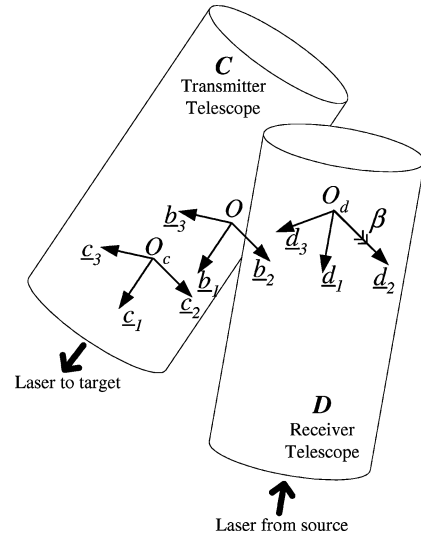
b) Bifocal relay mirror spacecraft

Fig. 1 Models used in the derivation of the equations of motion.

the center of mass of the overall spacecraft does not change during the motion of the VS-CMG around its gimbal.

In summary, Eq. (1) can be expressed as

$$\underline{h}_O = \underline{h}_B + \underline{h}_r + \underline{h}_g \qquad (4)$$

where $\underline{h}_B = \underline{J}_B \cdot \underline{\omega}$ is the total absolute angular momentum of the spacecraft, which is a combination of the contribution of the spacecraft's body inertia $\underline{J}_b$ and the inertia because the VS-CMG is not located at the spacecraft's center of mass.

The vectorial equation of motion for the overall spacecraft is

$$\dot{\underline{h}}_O = \underline{t}_e \qquad (5)$$

where the time derivative is in the inertial frame and $\underline{t}_e$ is the resultant vector of external torques.

The vectorial equations of motion of the VS-CMG rotor alone and of the overall VS-CMG (rotor plus gimbal) are

$$\dot{\underline{h}}_r = \underline{u}_r, \qquad \dot{\underline{h}}_r + \dot{\underline{h}}_g = \underline{u}_g \qquad (6)$$

where $\underline{u}_r$ is the total external torque acting on the VS-CMG rotor, including the control torque by the spin motor, directed as $\underline{a}_s$, and where $\underline{u}_g$ is the external torque acting on the VS-CMG, including the control torque by the gimbal motor, directed as $\underline{a}_g$.

To obtain the scalar equations of motion, each vectorial quantity is expressed in terms of its components with respect to a chosen reference frame. Using the vectrix notation, we can write

$$[\boldsymbol{h}_O \quad \boldsymbol{h}_B \quad \boldsymbol{h}_r \quad \boldsymbol{h}_g \quad \boldsymbol{h}_w \quad \boldsymbol{r}_w \quad \boldsymbol{\omega}]$$

$$= \mathbb{F}_b \cdot [\underline{\boldsymbol{h}}_O \quad \underline{\boldsymbol{h}}_B \quad \underline{\boldsymbol{h}}_r \quad \underline{\boldsymbol{h}}_g \quad \underline{\boldsymbol{h}}_w \quad \underline{\boldsymbol{r}}_w \quad \underline{\boldsymbol{\omega}}]$$

$$[\boldsymbol{\omega}_{\mathrm{gb}} \quad \boldsymbol{\omega}_{\mathrm{rg}}] = \mathbb{F}_g \cdot [\underline{\boldsymbol{\omega}}_{\mathrm{gb}} \quad \underline{\boldsymbol{\omega}}_{\mathrm{rg}}]$$

$$\boldsymbol{J}_b = \mathbb{F}_b \cdot \underline{\boldsymbol{J}}_b \cdot \mathbb{F}_b^T, \qquad \boldsymbol{J}_B = \mathbb{F}_b \cdot \underline{\boldsymbol{J}}_B \cdot \mathbb{F}_b^T$$

$$\boldsymbol{J}_r = \mathbb{F}_g \cdot \underline{\boldsymbol{J}}_r \cdot \mathbb{F}_g^T, \qquad \boldsymbol{J}_g = \mathbb{F}_g \cdot \underline{\boldsymbol{J}}_g \cdot \mathbb{F}_g^T \qquad (7)$$

where $\boldsymbol{h}_O \in \mathbb{R}^{3 \times 1}$ is the column matrix of the components of the vector $\underline{\boldsymbol{h}}_O$ along $\mathbb{F}_b$ and $\boldsymbol{J}_b \in \mathbb{R}^{3 \times 3}$ is the tensor of the moments of inertia, obtained by expression of the dyadic $\underline{\boldsymbol{J}}_b$ along $\mathbb{F}_b$, analogously for the other symbols.

By the introduction of relations (7) into the equation $\underline{\boldsymbol{h}}_B = \underline{\boldsymbol{J}}_B \cdot \underline{\boldsymbol{\omega}}$ and into Eq. (3) by multiplication on the left by $\mathbb{F}_b$ and by the use of the properties of the vectrix operator, the following scalar expressions are obtained:

$$\boldsymbol{h}_B = \boldsymbol{J}_B \boldsymbol{\omega} = \omega \left[\boldsymbol{J}_b + m_w \left(r_w^2 \boldsymbol{1} - \boldsymbol{r}_w \boldsymbol{r}_w^T \right) \right]$$

$$\boldsymbol{h}_r = \boldsymbol{C}_{\mathrm{bg}} \boldsymbol{J}_r \boldsymbol{C}_{\mathrm{gb}} \boldsymbol{\omega} + \boldsymbol{C}_{\mathrm{bg}} \boldsymbol{J}_r (\boldsymbol{\omega}_{\mathrm{gb}} + \boldsymbol{\omega}_{\mathrm{rg}})$$

$$\boldsymbol{h}_g = \boldsymbol{C}_{\mathrm{bg}} \boldsymbol{J}_g \boldsymbol{C}_{\mathrm{gb}} \boldsymbol{\omega} + \boldsymbol{C}_{\mathrm{bg}} \boldsymbol{J}_g \boldsymbol{\omega}_{\mathrm{gb}} \qquad (8)$$

where $\boldsymbol{C}_{\mathrm{bg}}$ is the rotation matrix from $\mathbb{F}_g$ to $\mathbb{F}_b$.

Let us now define the following relations:

$$\boldsymbol{\mu}_1 \triangleq [1 \quad 0 \quad 0]^T, \qquad \boldsymbol{\mu}_2 \triangleq [0 \quad 1 \quad 0]^T$$

$$\boldsymbol{\omega}_{\mathrm{rg}} \triangleq \boldsymbol{\mu}_1 \Omega, \qquad \boldsymbol{\omega}_{\mathrm{gb}} \triangleq \boldsymbol{\mu}_2 \dot{\delta}$$

$$\boldsymbol{C}_{\mathrm{bg}} \triangleq [\boldsymbol{a}_s \quad \boldsymbol{a}_g \quad \boldsymbol{a}_t], \qquad \boldsymbol{C}_{\mathrm{gb}} = \boldsymbol{C}_{\mathrm{bg}}^T \qquad (9)$$

with Ω being the spin angular speed of the VS-CMG rotor with respect to the gimbal and $\dot{\delta}$ being the angular speed of the overall VS-CMG with respect to the spacecraft body, around the gimbal axis $\underline{\boldsymbol{a}}_g$. Moreover, $\boldsymbol{a}_s$ is the column matrix of components along $\mathbb{F}_b$ of the basis vector $\underline{\boldsymbol{a}}_s$, that is, $\boldsymbol{a}_s = \mathbb{F}_b \cdot \underline{\boldsymbol{a}}_s$, analogously for $\underline{\boldsymbol{a}}_g$ and $\underline{\boldsymbol{a}}_t$. Inserting relations (8) into Eq. (4) and defining $\boldsymbol{J}_{(r+g)} \triangleq \boldsymbol{J}_r + \boldsymbol{J}_g$ as the inertia matrix of the overall VS-CMG, rotor and gimbal, along $\mathbb{F}_g$, we have

$$\boldsymbol{h}_O = \boldsymbol{J}_B \boldsymbol{\omega} + \left(\boldsymbol{C}_{\mathrm{bg}} \boldsymbol{J}_{(r+g)} \boldsymbol{C}_{\mathrm{gb}} \boldsymbol{\omega} + \boldsymbol{C}_{\mathrm{bg}} \boldsymbol{J}_{(r+g)} \boldsymbol{\mu}_2 \dot{\delta} + \boldsymbol{C}_{\mathrm{bg}} \boldsymbol{J}_r \boldsymbol{\mu}_1 \Omega \right) \quad (10)$$

Where the term in parentheses on the right-hand side is $\boldsymbol{h}_w$, expressing in $\mathbb{F}_b$ the absolute angular momentum of the overall VS-CMG.

Now, the scalar form of vectorial Eqs. (5) and (6), with reference of the terms to $\mathbb{F}_b$, becomes

$$\dot{\boldsymbol{h}}_O + \boldsymbol{\omega}^\times \boldsymbol{h}_O = \boldsymbol{t}_e \qquad (11)$$

$$\dot{\boldsymbol{h}}_r + \boldsymbol{\omega}^\times \boldsymbol{h}_r = \boldsymbol{u}_r \qquad (12)$$

$$\dot{\boldsymbol{h}}_r + \dot{\boldsymbol{h}}_g + \boldsymbol{\omega}^\times (\boldsymbol{h}_r + \boldsymbol{h}_g) = \boldsymbol{u}_g \qquad (13)$$

where the time derivatives are evaluated in $\mathbb{F}_b$ and superscript $\times$ indicates the matrix form of the vector product. Inserting Eq. (10) into Eq. (11), and taking into account that $\dot{\boldsymbol{C}}_{\mathrm{bg}} = \boldsymbol{C}_{\mathrm{bg}} \boldsymbol{\omega}_{\mathrm{gb}}^\times$, and $\dot{\boldsymbol{C}}_{\mathrm{gb}} = -\boldsymbol{\omega}_{\mathrm{gb}}^\times \boldsymbol{C}_{\mathrm{gb}}$, we find the equations of motion of the overall spacecraft with respect to the body frame with vectrix $\mathbb{F}_b$. It is convenient to write the equations in the following way, through the collection of the terms by factors of $\dot{\delta}$, $\ddot{\delta}$, Ω and $\dot{\Omega}$. Indeed, these variables can be directly measured and acted on at the VS-CMG level:

$$\boldsymbol{J}_1 \dot{\boldsymbol{\omega}} = [\boldsymbol{J}_1 \boldsymbol{\omega}]^\times \boldsymbol{\omega} - \boldsymbol{A}_1 \dot{\delta}^2 - \boldsymbol{B}_1 \ddot{\delta} - (\boldsymbol{D}_{11} + \boldsymbol{D}_{12} + \boldsymbol{D}_{13}) \dot{\delta}$$

$$- \boldsymbol{E}_1 \dot{\Omega} - \boldsymbol{F}_1 \Omega + \boldsymbol{t}_e \qquad (14)$$

where we defined

$$\boldsymbol{J}_1 \in \mathbb{R}^{3 \times 3} \triangleq \boldsymbol{J}_B + \boldsymbol{C}_{\mathrm{bg}} \boldsymbol{J}_{(r+g)} \boldsymbol{C}_{\mathrm{gb}}$$

$$\boldsymbol{A}_1 \in \mathbb{R}^{3 \times 1} \triangleq \boldsymbol{C}_{\mathrm{bg}} \boldsymbol{\mu}_2^\times \boldsymbol{J}_{(r+g)} \boldsymbol{\mu}_2 = -\boldsymbol{a}_t I_{(r+g)}^{12} + \boldsymbol{a}_s I_{(r+g)}^{23}$$

$$\boldsymbol{B}_1 \in \mathbb{R}^{3 \times 1} \triangleq \boldsymbol{C}_{\mathrm{bg}} \boldsymbol{J}_{(r+g)} \boldsymbol{\mu}_2 = \boldsymbol{a}_s I_{(r+g)}^{12} + \boldsymbol{a}_g I_{(r+g)}^{22} + \boldsymbol{a}_t I_{(r+g)}^{23}$$

$$\boldsymbol{D}_{11} \in \mathbb{R}^{3 \times 1} \triangleq \left(\boldsymbol{C}_{\mathrm{bg}} \boldsymbol{\mu}_2^\times \boldsymbol{J}_r \boldsymbol{\mu}_1 \right) \Omega = \left(-\boldsymbol{a}_t I_r^{11} + \boldsymbol{a}_s I_r^{13} \right) \Omega$$

$$\boldsymbol{D}_{12} \in \mathbb{R}^{3 \times 1} \triangleq -\boldsymbol{B}_1^\times \boldsymbol{\omega}$$

$$\boldsymbol{D}_{13} \in \mathbb{R}^{3 \times 1} \triangleq \left(\boldsymbol{C}_{\mathrm{bg}} \boldsymbol{\mu}_2^\times \boldsymbol{J}_{(r+g)} \boldsymbol{C}_{\mathrm{gb}} - \boldsymbol{C}_{\mathrm{bg}} \boldsymbol{J}_{(r+g)} \boldsymbol{\mu}_2^\times \boldsymbol{C}_{\mathrm{gb}} \right) \boldsymbol{\omega}$$

$$= \left[\left(\bar{\boldsymbol{C}} \boldsymbol{J}_{(r+g)} \boldsymbol{C}_{\mathrm{gb}} \right) + \left(\bar{\boldsymbol{C}} \boldsymbol{J}_{(r+g)} \boldsymbol{C}_{\mathrm{gb}} \right)^T \right] \boldsymbol{\omega}$$

$$\boldsymbol{E}_1 \in \mathbb{R}^{3 \times 1} \triangleq \boldsymbol{C}_{\mathrm{bg}} \boldsymbol{J}_r \boldsymbol{\mu}_1 = \boldsymbol{a}_s I_r^{11} + \boldsymbol{a}_g I_r^{12} + \boldsymbol{a}_t I_r^{13}$$

$$\boldsymbol{F}_1 \in \mathbb{R}^{3 \times 1} \triangleq -\boldsymbol{E}_1^\times \boldsymbol{\omega} \qquad (15)$$

where $\bar{\boldsymbol{C}} \triangleq [-\boldsymbol{a}_t \quad \boldsymbol{0} \quad \boldsymbol{a}_s]$ and $I_{(r+g)}^{ij}$ and I_r^{ij} indicate the elements (i, j) of the inertia matrices $\boldsymbol{J}_{(r+g)}$ and $\boldsymbol{J}_r$. All of the matrices just defined depend, in general, on the gimbal position δ because both $\boldsymbol{a}_s$ and $\boldsymbol{a}_t$ depend on δ. In particular, the magnitude of $\boldsymbol{D}_{11}$ is the gain of the torque amplification effect of the VS-CMG, and it usually becomes much larger than the other factors when the VS-CMG is moved around its gimbal.

The matrix factors $\boldsymbol{B}_1^\times$ in $\boldsymbol{D}_{12}$ and $\boldsymbol{E}_1^\times$ in $\boldsymbol{F}_1$ are antisymmetric by definition of the operator superscript $\times$. The matrix factor of $\boldsymbol{\omega}$ in $\boldsymbol{D}_{13}$ is symmetric because it is the sum of a matrix with its transpose, but its sign is, in general, indefinite. These statements are of interest in relation to control law design. The term depending on $\dot{\delta}^2$ in Eq. (14) does not appear in the equations of Ref. 6; however, the matrix factor $\boldsymbol{A}_1$ is, in general, not null.

The equations of the motion of the rotor around the spin axis $\underline{\boldsymbol{a}}_s$ and of the overall VS-CMG around the gimbal axis $\underline{\boldsymbol{a}}_g$ are obtained by the projection of Eqs. (12) and (13) along those two axes

$$I_r^{11} \left(\dot{\Omega} + \boldsymbol{a}_s^T \dot{\boldsymbol{\omega}} \right) + I_r^{12} \left(\ddot{\delta} + \boldsymbol{a}_g^T \dot{\boldsymbol{\omega}} \right) + I_r^{13} \left(\Omega \dot{\delta} + \boldsymbol{a}_t^T \dot{\boldsymbol{\omega}} \right) + I_r^{23} \dot{\delta}^2$$

$$+ \boldsymbol{a}_s^T \left\{ -[(\boldsymbol{C}_{\mathrm{bg}} \boldsymbol{J}_r \boldsymbol{C}_{\mathrm{gb}}) \boldsymbol{\omega}]^\times \boldsymbol{\omega} + (\boldsymbol{D}_{r12} + \boldsymbol{D}_{r13}) \dot{\delta} + \boldsymbol{F}_1 \Omega \right\} = \boldsymbol{a}_s^T \boldsymbol{u}_r$$

$$I_{(r+g)}^{22} \left(\ddot{\delta} + \boldsymbol{a}_g^T \dot{\boldsymbol{\omega}} \right) + I_{(r+g)}^{12} \boldsymbol{a}_s^T \dot{\boldsymbol{\omega}} + I_{(r+g)}^{23} \boldsymbol{a}_t^T \dot{\boldsymbol{\omega}} + I_r^{12} \dot{\Omega}$$

$$+ \boldsymbol{a}_g^T \left\{ -\left[(\boldsymbol{C}_{\mathrm{bg}} \boldsymbol{J}_{(r+g)} \boldsymbol{C}_{\mathrm{gb}}) \boldsymbol{\omega} \right]^\times \boldsymbol{\omega} + (\boldsymbol{D}_{12} + \boldsymbol{D}_{13}) \dot{\delta} + \boldsymbol{F}_1 \Omega \right\} = \boldsymbol{a}_g^T \boldsymbol{u}_g$$

$$(16)$$

where $\boldsymbol{D}_{r12}$ and $\boldsymbol{D}_{r13}$ are obtained from the $\boldsymbol{D}_{12}$ and $\boldsymbol{D}_{13}$ defined in Eqs. (15) when $\boldsymbol{J}_{(r+g)}$ is replaced with $\boldsymbol{J}_r$.

B. Rigid Body with N VS-CMGs

In this section, the preceding analytical model is extended to the case of a rigid-body spacecraft with N VS-CMGs in a generic configuration. Start from Eqs. (10) and sum the contribution of each VS-CMG; then the total angular momentum becomes

$$\boldsymbol{h}_O = \boldsymbol{J}_{BN} \boldsymbol{\omega} + \sum_{i=1}^{N} \left(\boldsymbol{C}_{\mathrm{bg}i} \boldsymbol{J}_{(r+g)i} \boldsymbol{C}_{\mathrm{bg}i}^T \boldsymbol{\omega} \right.$$

$$\left. + \boldsymbol{C}_{\mathrm{bg}i} \boldsymbol{J}_{(r+g)i} \boldsymbol{\mu}_2 \dot{\delta}_i + \boldsymbol{C}_{\mathrm{bg}i} \boldsymbol{J}_{ri} \boldsymbol{\mu}_1 \Omega_i \right) \qquad (17)$$

where it has been defined

$$\boldsymbol{J}_{BN} \triangleq \boldsymbol{J}_b + \sum_{i=1}^{N} m_{wi} \left(r_{wi}^2 \boldsymbol{1} - \boldsymbol{r}_{wi} \boldsymbol{r}_{wi}^T \right) \qquad (18)$$

By insertion of $\boldsymbol{h}_O$ given by Eq. (17) into Eq. (11), the equations of the motion of the overall spacecraft with N VS-CMGs, written in a

compact form, become

$$J_N\dot{\boldsymbol{\omega}} = [J_N\boldsymbol{\omega}]^\times\boldsymbol{\omega} - A\dot{\boldsymbol{\Delta}}^2 - B\ddot{\boldsymbol{\Delta}} - (D_1 + D_2 + D_3)\dot{\boldsymbol{\Delta}}$$

$$- E\dot{\boldsymbol{\Omega}} - F\boldsymbol{\Omega} + t_e \qquad (19)$$

where we defined

$$J_N \in \mathbb{R}^{3\times 3} \triangleq J_{BN} + \sum_{i=1}^{N} C_{\mathrm{bg}i} J_{(r+g)i} C_{\mathrm{gb}i}$$

$$A \in \mathbb{R}^{3\times N} \triangleq [A_1 \quad \cdots \quad A_N]$$

$$\dot{\boldsymbol{\Delta}}^2 \in \mathbb{R}^{N\times 1} \triangleq \begin{bmatrix} \dot{\delta}_1^2 & \cdots & \dot{\delta}_N^2 \end{bmatrix}^T$$

$$\boldsymbol{\Delta} \in \mathbb{R}^{N\times 1} \triangleq [\delta_1 \quad \cdots \quad \delta_N]^T$$

$$B \in \mathbb{R}^{3\times N} \triangleq [B_1 \quad \cdots \quad B_N]$$

$$D_i \in \mathbb{R}^{3\times N} \triangleq [D_{1i} \quad \cdots \quad D_{Ni}], \qquad i = 1, 2, 3$$

$$E \in \mathbb{R}^{3\times N} \triangleq [E_1 \quad \cdots \quad E_N]$$

$$\Omega \in \mathbb{R}^{N\times 1} \triangleq [\Omega_1 \quad \cdots \quad \Omega_N]^T$$

$$F \in \mathbb{R}^{3\times N} \triangleq [F_1 \quad \cdots \quad F_N] \qquad (20)$$

and the definitions in Eqs. (15) are used to obtain the elements of the matrices A, B, D, E, and F, along with the specific values of C_{bg}, $J_{(r+g)}$, and J_r for each VS-CMG.

Equations (16) still apply for each one of the N VS-CMGs.

C. Dual-Body Spacecraft with N VS-CMGs

Finally, in this section, we develop the equations of motion of a dual-body spacecraft with N VS-CMGs, as represented in Fig. 1b. The bodies C and D, in this conceptual model, represent the transmitter and the receiver telescopes of a spacecraft for the relay of optical signals. The receiver telescope rotates with respect to the transmitter around an axis that contains, as a design hypothesis, the center of mass of the receiver telescope itself; therefore, the center of mass of the overall system does not change during the relative rotation. In Fig. 1b, points O_c, O_d, and O are, respectively, the center of mass of the transmitter telescope, the receiver telescope, and the overall spacecraft. A frame with vectrix $\mathbb{F}_c$ is fixed with respect to the transmitter telescope: Here, $\underline{c}_1$ is the optical axis of the telescope and $\underline{c}_2$ is parallel to the rotation axis between the two telescopes. A frame with vectrix $\mathbb{F}_d$ is fixed with respect to the receiver telescope: In this case, $\underline{d}_1$ is the optical axis of the receiver telescope and $\underline{d}_2$ is the relative rotation axis. $\mathbb{F}_d$ is rotated with respect to $\mathbb{F}_c$ of an angle β around $\underline{d}_2$. Finally, $\mathbb{F}_b$ is parallel to $\mathbb{F}_c$, but centered in the center of mass of the overall spacecraft. The transmitter telescope is supposed to contain N single-gimbal VS-CMGs, not shown in Fig. 1b.

In summary, our dynamic model has a total of $(2N + 7)$ degrees of freedom (DOF): three DOF for the position of the center of mass of the system, three DOF for the attitude of the transmitter telescope, one DOF for the relative angular displacement of the telescopes, and two DOF for the gimbal and rotor position of each VS-CMG.

To write the equations of motion for this system, we add the contribution of the steerable receiver telescope to the angular momentum of the single-body case. We first write the absolute vectorial angular momentum of the receiver telescope with respect to O_d:

$$\underline{h}_d = \underline{J}_d \cdot \underline{\omega}_d = \underline{J}_d \cdot (\underline{\omega} + \underline{\omega}_{db}) \qquad (21)$$

with $\underline{\omega}_d$ being the absolute angular velocity of the receiver telescope, $\underline{J}_d$ the inertia dyadic of the receiver telescope with respect to its center of mass, and $\underline{\omega}_{db}$ the relative angular velocity of the receiver telescope with respect to the transmitter.

The vectorial equation of motion of the receiver telescope alone is

$$\underline{\dot{h}}_d = \underline{u}_d \qquad (22)$$

where $\underline{u}_d$ is the total external torque acting on the receiver, including the control torque exerted by the motor between the two telescopes, directed as $\underline{d}_2$.

By the expression of each vector quantity of Eq. (21) with respect to a suitable reference frame,

$$h_d = \mathbb{F}_b \cdot \underline{h}_d, \qquad \omega_{db} = \mathbb{F}_d \cdot \underline{\omega}_{db}, \qquad J_d = \mathbb{F}_d \cdot \underline{J}_d \cdot \mathbb{F}_d^T \quad (23)$$

and by the definition of

$$\omega_{db} \triangleq \mu_2 \dot{\beta}, \qquad C_{bd} \triangleq [d_1 \quad \mu_2 \quad d_3], \qquad C_{db} = C_{bd}^T \qquad (24)$$

the following expression yields

$$h_d = (C_{bd} J_d C_{db})\,\omega + C_{bd} J_d \mu_2 \dot{\beta} \qquad (25)$$

The total angular momentum is obtained when h_d is appended from Eq. (25), on the right-hand side of Eq. (17) and also when the transport inertia terms due to the masses of the two telescopes are taken into account. By insertion of the total angular momentum into Eq. (11), the three equations of motion of the overall dual-body system are found:

$$J_{\mathrm{tot}}\dot{\boldsymbol{\omega}} = [J_{\mathrm{tot}}\boldsymbol{\omega}]^\times\boldsymbol{\omega} - A\dot{\boldsymbol{\Delta}}^2 - B\ddot{\boldsymbol{\Delta}} - (D_1 + D_2 + D_3)\dot{\boldsymbol{\Delta}}$$

$$- E\dot{\boldsymbol{\Omega}} - F\boldsymbol{\Omega} + t_e - A_d\dot{\beta}^2 - B_d\ddot{\beta} - (D_{d2} + D_{d3})\,\dot{\beta} \qquad (26)$$

where A_d, B_d, D_{d2}, and D_{d3} are obtained from the A_1, B_1, D_{12}, and D_{13}, defined in Eqs. (15), by the replacement of C_{bg} with C_{bd} and $J_{(r+g)}$ with J_d. In addition to the definitions in Eqs. (20), we define

$$J_{\mathrm{tot}} \in \mathbb{R}^{3\times 3} \triangleq J_N + m_c\left(r_c^2 \mathbf{1} - r_c r_c^T\right)$$

$$+ m_d\left(r_d^2 \mathbf{1} - r_d r_d^T\right) + (C_{bd} J_d C_{db}) \qquad (27)$$

where m_c and m_d are, respectively, the mass of the transmitter and of the receiver telescopes and $r_c = \mathbb{F}_b \cdot O_c - O$ and $r_d = \mathbb{F}_b \cdot O_d - O$.

Moreover, the equation of motion of the overall receiver telescope around the gimbal axis $\underline{d}_2$ is given by

$$I_d^{22}\left(\ddot{\beta} + \mu_2^T \dot{\boldsymbol{\omega}}\right) + I_d^{12} d_1^T \dot{\boldsymbol{\omega}} + I_d^{23} d_3^T \dot{\boldsymbol{\omega}}$$

$$+ \mu_2^T\left\{-[(C_{bd} J_d C_{db})\omega]^\times \omega + (D_{d2} + D_{d3})\dot{\beta}\right\} = u_d \qquad (28)$$

where I_d^{ij} indicates the element (i, j) of the inertia matrix J_d and u_d, aside from the friction, is the torque acting on the receiver telescope due to the joint motor between the two telescopes. Equations (26) and (28), along with Eqs. (16) for each VS-CMG, completely describe the rotational dynamics of our model.

Note that the contribution of the receiver telescope to the equations of motion is analogous to the contribution of a single-gimbal CMG with the inertia and mass characteristics of the receiver telescope and fixed rotor.

III. Determination of the Reference Maneuver

This section outlines the determination of the reference attitude and joint motion for the dual-body spacecraft modeled earlier, given its orbital parameters and the ground positions of the laser source and the target, which receiver and transmitter telescopes must simultaneously track. The ground laser source is supposed to be cooperative and track the receiver telescope of the satellite. The computed reference motion is used, in our simulations, to guide the spacecraft during the tracking control.

These simplifying hypotheses are considered: Both target and source are fixed on the Earth's surface; the Earth is spherical; moreover, $O_c \equiv O \equiv O_d$ (Fig. 1b).

The following four geometry conditions must be satisfied for the relay mission:

$$\underline{c}_1 = (L_{tg} - O)/|L_{tg} - O|, \qquad \underline{d}_1 = (L_{sr} - O)/|L_{sr} - O|$$
$$\beta = \arccos(\underline{c}_1 \cdot \underline{d}_1), \qquad \underline{d}_2 = (\underline{c}_1 \times \underline{d}_1)/|\underline{c}_1 \times \underline{d}_1| \quad (29)$$

Because of the first two conditions, the telescopes optical axes cross the target and source points (L_{tg} and L_{sr}); the third condition imposes that the joint angle be equal to the angular separation between the target and the source, as seen at the spacecraft location; and the fourth condition imposes that the rotation axis $\underline{d}_2$ between the two telescopes be perpendicular to the plane defined by the locations of the spacecraft, the target point, and the source point.

The following algorithmic steps are conducted to obtain the reference spacecraft attitude and the joint angle at discrete points along the relay portion of the spacecraft orbit, that is, the portion of the orbit at which both the source and the target are visible: 1) Calculate the position of the source and the target in the Earth celestial frame (ECF), starting from their known positions in the Earth geographic frame. 2) Deduce the current position of the spacecraft and the subsatellite point in the ECF, starting from the orbital parameters. 3) Impose the conditions of Eqs. (29). 4) Express the attitude of the frame with vectrix $\mathbb{F}_b$ with respect to the spacecraft celestial frame.

By repeating the preceding algorithm at regular time steps, the reference sequence of the Euler's parameters and the joint angle values is finally obtained. Useful equations to implement this algorithm can be found in Ref. 15.

IV. Design of the Control Law

This section introduces the feedback control law for large rotational maneuvers of the dual-body spacecraft with N VS-CMGs, as modeled earlier. The new nonlinear feedback law proposed here is an extended and improved version of the law proposed in Ref. 6 and used as a base in Ref. 7. The feedback law is extended to enforce the regulation of the additional state variable β, which is the angle between the two telescopes. Moreover, the feedback law is improved by exploitation of the antisymmetry of some of the matrix factors of the equations of motion, already discussed in Sec. II.A.

Lyapunov's direct method is used for the control law design. It is assumed that estimates of the current state variables of the system (ω, q, $\dot{\beta}$, β, Ω, and Δ) are available in real time, where q are the Euler's parameters.

The target state is given by ω_f, q_f, $\dot{\beta}_f$, and β_f, with free values of Δ and Ω. Let V be the following Lyapunov's function:

$$V = k_q \Delta q^T \Delta q + \tfrac{1}{2}\Delta\omega^T J_{\text{tot}}\Delta\omega + \tfrac{1}{2}I_d^{22}(\Delta\dot{\beta})^2 + \tfrac{1}{2}k_{p\beta}(\Delta\beta)^2 \quad (30)$$

where k_q and $k_{p\beta}$ are positive constants and we defined the error term $\Delta q \triangleq (q - q_f)$, analogously for $\Delta\omega$, $\Delta\dot{\omega}$, $\Delta\beta$, $\Delta\dot{\beta}$, and $\Delta\ddot{\beta}$.

The time derivative of V can be written as

$$\dot{V} = 2k_q\Delta\dot{q}^T\Delta q + \Delta\omega^T J_{\text{tot}}\Delta\dot{\omega} + \tfrac{1}{2}\Delta\omega^T\dot{J}_{\text{tot}}\Delta\omega$$
$$+ I_d^{22}\Delta\dot{\beta}\Delta\ddot{\beta} + k_{p\beta}\Delta\dot{\beta}\Delta\beta \quad (31)$$

Now, let us execute the following steps: 1) The relation between the Euler's parameters and the angular velocity (as in Ref. 14)

$$\dot{q} = \tfrac{1}{2}Q(q)\omega \quad (32)$$

is substituted into the first term on the right-hand side of Eq. (31). 2) The expression of $\dot{\omega}$ from Eq. (26) is substituted into the second term of Eq. (31). 3) The time derivative of J_{tot}, as defined in Eq. (27), is substituted into the third term of Eq. (31). 4) The expression of $\ddot{\beta}$ from Eq. (28) is substituted into the fourth term of Eq. (31).

Finally, after some algebraic steps, we have

$$\dot{V} = -\Delta\omega^T\big\{k_q Q(q)^T q_f + J_{\text{tot}}\dot{\omega}_f - [J_{\text{tot}}\omega]^\times\omega_f + A\dot{\Delta}^2 + B\ddot{\Delta}$$
$$+ D\dot{\Delta} + E\dot{\Omega} + F_f\Omega - t_e + A_d\dot{\beta}^2 + B_d\ddot{\beta} + D_d\dot{\beta}\big\}$$
$$- \Delta\dot{\beta}\big\{-k_{p\beta}\Delta\beta + I_d^{22}(\ddot{\beta}_f + \mu_2^T\dot{\omega}) + I_d^{12}d_1^T\dot{\omega} + I_d^{23}d_3^T\dot{\omega}$$
$$+ \mu_2^T\big[-[(C_{bd}J_dC_{db})\omega]^\times\omega + (D_{d2} + D_{d3})\dot{\beta}\big] - u_d\big\} \quad (33)$$

where it has been defined

$$D \triangleq [D_1 + D_{2f} + (D_3 + D_{3f})/2]$$
$$D_d \triangleq [D_{d2f} + (D_{d3} + D_{d3f})/2] \quad (34)$$

and the matrices $F_f, D_{2f}, D_{3f}, D_{d2f}$, and D_{d3f} are obtained from the matrices F, D_2, D_3, D_{d2}, and D_{d3} defined in Eqs. (20) and (26) by the replacement of ω with ω_f. The antisymmetry of the matrix factor $[J_{\text{tot}}\omega]^\times$ has been exploited in Eq. (33) to replace the term $[J_{\text{tot}}\omega]^\times\omega$ with $[J_{\text{tot}}\omega]^\times\omega_f$. (In fact, $[J_{\text{tot}}\omega]^\times\omega = [J_{\text{tot}}\omega]^\times\Delta\omega + [J_{\text{tot}}\omega]^\times\omega_f$, and $\Delta\omega^T[J_{\text{tot}}\omega]^\times\Delta\omega = 0$.) For the same reason, the terms F, D_2, D_3, D_{d2}, and D_{d3} have been replaced with $F_f, D_{2f}, D_{3f}, D_{d2f}$, and D_{d3f}. These substitutions are advantageous because ω_f is perfectly known, whereas ω is, in practice, estimated and affected by bias and noise. Moreover, the control laws, in case of regulation, becomes simpler.

Equation (33), when the terms in the braces on the right-hand side are condensed to $\{R_1\}$ and $\{R_2\}$ for convenience, becomes

$$\dot{V} = -\Delta\omega^T\{R_1\} - \Delta\dot{\beta}\{R_2\} \quad (35)$$

For $\dot{V}$ to be negative semidefinite, it is sufficient that the following two conditions are satisfied:

$$\{R_1\} = K\Delta\omega, \qquad \{R_2\} = k_{d\beta}\Delta\dot{\beta} \quad (36)$$

where K is a positive definite gain matrix and $k_{d\beta}$ is a positive constant gain.

Equations (36) can be rearranged when the control terms of the system are moved to the left-hand sides:
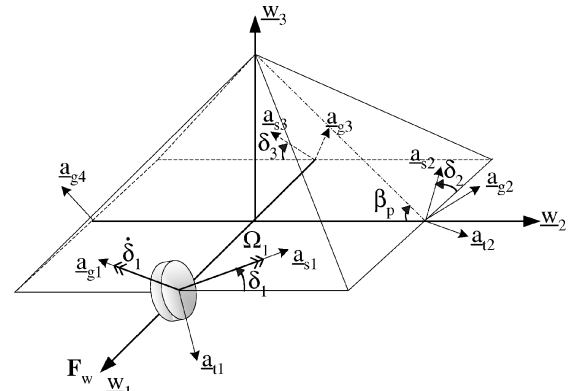
$$B\ddot{\Delta} + D\dot{\Delta} + E\dot{\Omega} = t_{\text{req}}, \qquad u_d = u_{d\,\text{req}} \quad (37)$$

with

$$t_{\text{req}} = K\Delta\omega - k_q Q(q)^T q_f - J_{\text{tot}}\dot{\omega}_f + [J_{\text{tot}}\omega]^\times\omega_f - A\dot{\Delta}^2$$
$$- F_f\Omega + t_e - A_d\dot{\beta}^2 - B_d\ddot{\beta} - D_d\dot{\beta}$$
$$u_{d\,\text{req}} = -k_{d\beta}\Delta\dot{\beta} - k_{p\beta}\Delta\beta + I_d^{22}(\ddot{\beta}_f + \mu_2^T\dot{\omega}) + I_d^{12}d_1^T\dot{\omega} + I_d^{23}d_3^T\dot{\omega}$$
$$+ \mu_2^T\big[-[(C_{bd}J_dC_{db})\omega]^\times\omega + (D_{d2} + D_{d3})\dot{\beta}\big] \quad (38)$$

Table 1   Values of geometric and mass parameters used in simulations

Parameter	Value
J_c (transmitter inertia)	diag[882, 2997, 3164], kg·m^2
J_d (receiver inertia)	diag[183, 1721, 1560], kg·m^2
m_c (transmitter mass)	2267, kg
m_d (receiver mass)	973, kg
r_c ($\mathbb{F}_b \cdot O_c - O$ in Fig. 1b)	$[-0.27, -0.49, 0]^T$, m
r_d ($\mathbb{F}_b \cdot \overline{O_d - O}$ in Fig. 1b)	$[0.63, 1.15, 0]^T$, m
β_p (Fig. 2)	54.74, deg
$J_{(r+g)}$ (VS-CMG total inertia)	diag[0.27, 0.135, 0.135], kg·m^2
J_r (VS-CMG rotor inertia)	diag[0.245, 0.1, 0.1], kg·m^2

Fig. 2   Cluster of four single-gimbal CMGs in a pyramid configuration.

a) Spacecraft angular velocity

b) Spacecraft attitude (Euler's parameter)

c) Spacecraft joint angle and torque

d) Actuator spin rates

e) Actuator gimbal rates

f) Actuator gimbal angles

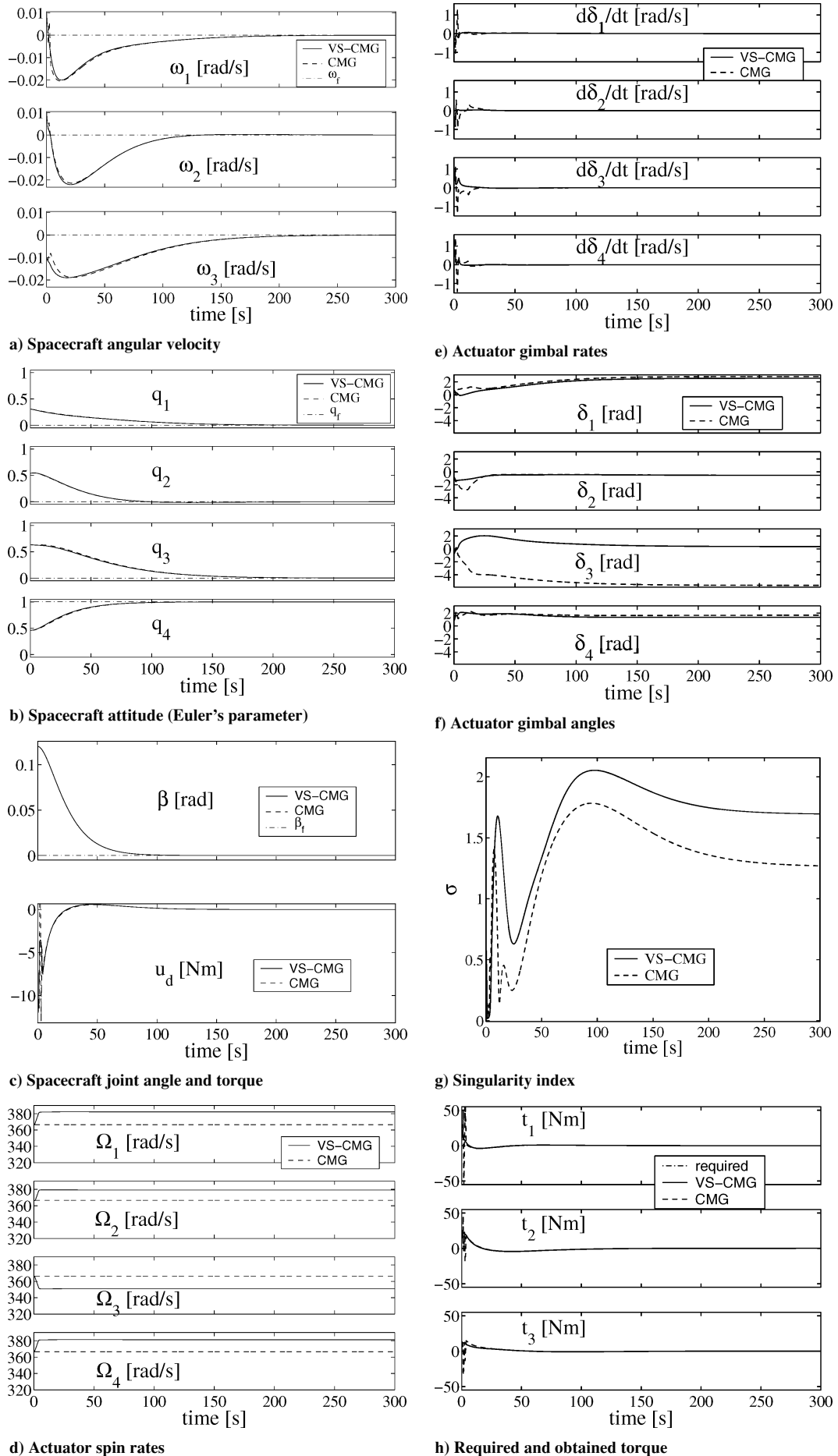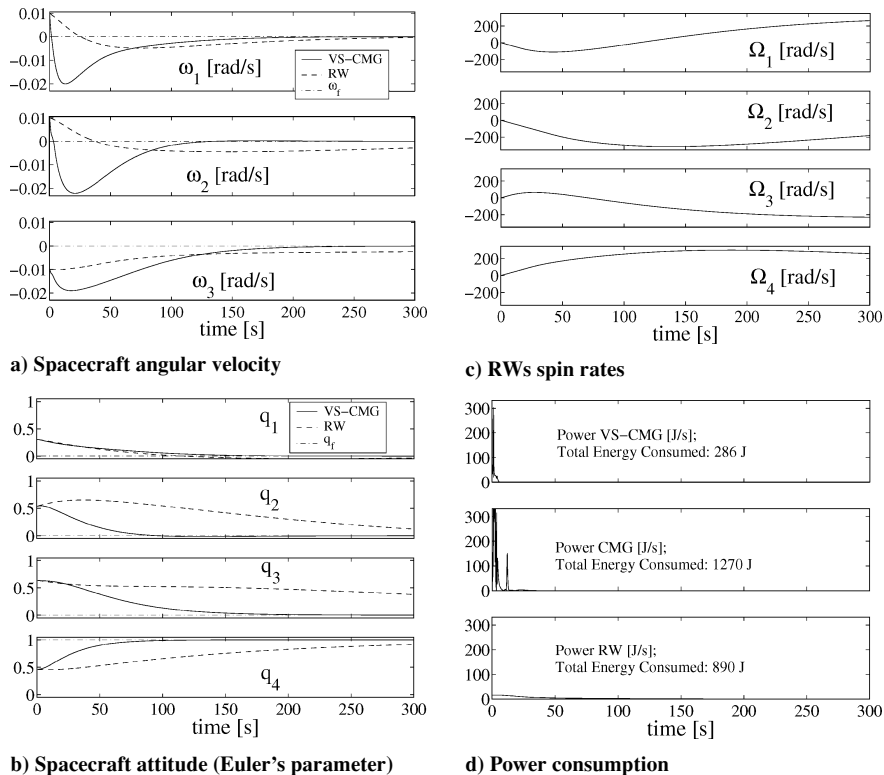g) Singularity index

h) Required and obtained torque

Fig. 3   Results of case 1 (regulation control); use of VS-CMGs compared to use of CMGs.

Table 2   Values of control law, steering law, and saturation parameters used in simulations

Parameter	Case	Value
k_q (see Eq. 38)	Regulation VS-CMGs/CMGs	$35 \text{ N} \cdot \text{m}$
	Regulation RWs	$1.75 \text{ N} \cdot \text{m}$
	Tracking	$10^4 \text{ N} \cdot \text{m}$
$\boldsymbol{K}$ (see Eq. 38)	Regulation VS-CMGs/CMGs	$\text{diag}[616, 705, 881] \text{ N} \cdot \text{m} \cdot \text{s}$
	Regulation RWs	$\text{diag}[138, 158, 197] \text{ N} \cdot \text{m} \cdot \text{s}$
	Tracking	$\text{diag}[10417, 11914, 14895] \text{ N} \cdot \text{m} \cdot \text{s}$
$k_{p\beta}$ (see Eq. 38)	Regulation	$10 \text{ N} \cdot \text{m}$
	Tracking	$10^3 \text{ N} \cdot \text{m}$
$k_{d\beta}$ (see Eq. 38)	Regulation	$262.4 \text{ N} \cdot \text{m} \cdot \text{s}$
	Tracking	$2624 \text{ N} \cdot \text{m} \cdot \text{s}$
$k_{\hat{\delta}}$ (see Eq. 43)	Regulation/tracking	50 s^{-1}
w_g (see Eq. 44)	Regulation/tracking	1.0
w_{s0} (see Eq. 44)	Regulation/tracking	1.0
μ (see Eq. 44)	Regulation/tracking	10^{-2}
α_0 (see Eq. 45)	Regulation/tracking	10^{-1}
$|\boldsymbol{\Delta}|_{\max}$	Regulation/tracking	$5 \cdot [1, 1, 1, 1]^T \text{ rad/s}$
$|\dot{\boldsymbol{\Delta}}|_{\max}$	Regulation/tracking	$2 \cdot [1, 1, 1, 1]^T \text{ rad/s}^2$
$|\boldsymbol{\Omega}|_{\max}$	Regulation/tracking	$628 \cdot [1, 1, 1, 1]^T \text{ rad/s}$
$|\dot{\boldsymbol{\Omega}}|_{\max}$	Regulation/tracking	$4 \cdot [1, 1, 1, 1]^T \text{ rad/s}^2$

Table 3   Values of initial and target conditions used in simulations

Parameter	Case	Value
$\boldsymbol{\Omega}_0$ (rotor rates)	VS-CMGs/CMGs	$366.5 \cdot [1, 1, 1, 1]^T \text{ rad/s}$
	RWs	$[0, 0, 0, 0]^T \text{ rad/s}$
$\boldsymbol{\Delta}_0$ (gimbal angles)	Regulation VS-CMGs/CMGs	$\pi/4 \cdot [1, -1, -1, 1]^T \text{ rad}$
	tracking VS-CMGs/CMGs	$[0, 0, 0, 0]^T \text{ rad}$
	Regulation/tracking RWs	$\pi/2 \cdot [1, 1, 1, 1]^T \text{ rad}$
$\dot{\boldsymbol{\Delta}}_0$ (gimbal rates)	Regulation/tracking	$[0, 0, 0, 0]^T \text{ rad/s}$
$\boldsymbol{\omega}_0$ (angular velocity)	Regulation	$[0.01, 0.01, -0.01]^T \text{ rad/s}$
	Tracking	$[0, 0, 0]^T \text{ rad/s}$
$\boldsymbol{q}_0$ (attitude)	Regulation	$[0.31, 0.54, 0.64, 0.46]^T$
	Tracking	$[0, 0, 0, 1]^T$
β_0 (joint angle)	Regulation	0.12 rad
	Tracking	0.4037 rad
$\boldsymbol{\omega}_f$ (reference angle velocity)	regulation	$[0, 0, 0]^T \text{ rad/s}$
$\boldsymbol{q}_f$ (reference attitude)	Regulation	$[0, 0, 0, 1]^T$
β_f (reference joint angle)	Regulation	0 rad

a) Spacecraft angular velocity

c) RWs spin rates

b) Spacecraft attitude (Euler's parameter)

d) Power consumption

Fig. 4   Results of case 1 (regulation control); use of VS-CMGs compared to use of RWs.

These are the designed control laws. Because they satisfy Eqs. (37) and (38), the derivative of the Lyapunov's function is negative semidefinite and the target state becomes asymptotically stable (as demonstrated hereafter) for the closed-loop system.

The second equation of the control laws in Eqs. (37) has a feedback-linearization effect[16] on the closed-loop system. Indeed, by placement of the torques $u_{d\text{req}}$ given by Eq. (38) into the equation of motion (28), the following equation is obtained for the error dynamics:

$$I_d^{22} \Delta\ddot{\beta} + k_{d\beta}\Delta\dot{\beta} + k_{p\beta}\Delta\beta = 0 \tag{39}$$

This is an unforced second-order system in the error terms. The constant $k_{d\beta}$ can be chosen to be equal to $2\sqrt{(I_d^{22}k_{p\beta})}$ to guarantee a critically damped behavior of the error term. The constant $k_{p\beta}$ can be chosen based on the maximum available torque and the set saturation error. A similar case applies to the first equation of the control laws (37), which affords a choice of the constant K, as in Ref. 6.

Interestingly, in the case of regulation control ($\omega_f = 0$), the first equation of Eq. (38) simplify to

$$t_{\text{req}} = K\omega - k_q Q(q)^T q_f - A\dot{\Delta}^2 + t_e - A_d\dot{\beta}^2 - B_d\ddot{\beta} - (D_{d3}/2)\dot{\beta} \tag{40}$$

A. Demonstration of Asymptotic Stability

$\dot{V}$ is semidefinite negative in the domain containing the variable states errors $\Delta\omega$, Δq, $\Delta\dot{\beta}$, and $\Delta\beta$; in fact, $\dot{V}$ does not depend explicitly on Δq and $\Delta\beta$, as in Eq. (35). Then the direct Lyapunov's theorem guarantees only the stability of the closed-loop system for all of the states errors, but not the asymptotic stability.

The global asymptotic stability of the closed-loop system can be demonstrated practically by showing that the only equilibrium point for V is at the target state. However, a more formal demonstration is shown hereafter, as in Ref. 7. In particular, a sufficient condition for asymptotic stability is that the first higher-order derivative of V, which is nonzero in the set Z of states where $\dot{V}$ is zero, must be of odd order and be negative definite in Z (Ref. 17). In our case, Z is the set of zero values for $\Delta\omega$ and $\Delta\dot{\beta}$ and arbitrary values for Δq and $\Delta\beta$, as in Eqs. (35) and (36). The second derivative of V (when the control law is applied) is still zero in the set Z:

$$\frac{d^2V}{dt^2} = -2\Delta\omega^T K\Delta\dot{\omega} - 2\Delta\dot{\beta}k_{d\beta}\Delta\ddot{\beta} \tag{41}$$

By the use of the time derivative of Eq. (41) and by consideration of Eqs. (26), (28), and (36), after some algebraic steps, the third derivative of V in Z is written as

$$\frac{d^3V}{dt^3} = -2k_q^2 q_f^T Q(q)\left(J_{\text{tot}}^{-1}\right)^T K J_{\text{tot}}^{-1} Q(q)^T q_f - 2k_{d\beta}\frac{k_{p\beta}^2}{I_d^{22}}(\Delta\beta)^2 \tag{42}$$

which is negative definite. In fact, J_{tot} and K are positive-definite matrices, and $k_{d\beta}$ and $k_{p\beta}$ are positive constants. Moreover, $q_f^T Q(q) = [Q(q)^T q_f]^T$, and this quantity is equal to zero only when $\Delta q = 0$. Therefore, the asymptotic stability of the closed-loop system is proved.

B. Steering Laws for the VS-CMGs and CMGs

The first control law in Eqs. (37) and (38) does not contain the physical control torques of the gimbals and rotors explicitly. Only gimbal and rotor accelerations and gimbal rates appear. To satisfy the control law, a steering law is typically exploited. From the required torque, the steering law determines the required value of $\dot{\Omega}$ and the required value of either $\dot{\Delta}$ (gimbal rate steering law) or $\ddot{\Delta}$ (gimbal acceleration steering law). The rotor and gimbal motors are then commanded to track these required values.

In our simulations, an acceleration steering law was used. In fact, this provides more realistic results than the rate steering law because it takes into account the inertia around the gimbal axes and allows for the computation of the power consumption.

In particular, for the case of VS-CMGs, we used a modified version of the acceleration steering law introduced in Ref. 7, which the reader is referred to for a detailed explanation. The law is given by
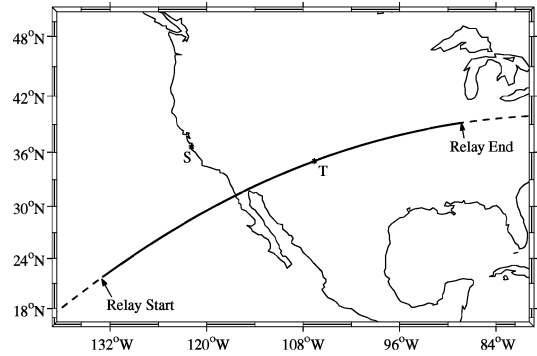
$$\begin{bmatrix} \dot{\Omega} \\ \ddot{\Delta} \end{bmatrix} = \begin{bmatrix} 1 & 0 \\ 0 & k_{\delta}1 \end{bmatrix} \left\{ WQ^T(QWQ^T)^{-1}t_{\text{req}} - \begin{bmatrix} 0 \\ \dot{\Delta} \end{bmatrix} \right\} \tag{43}$$

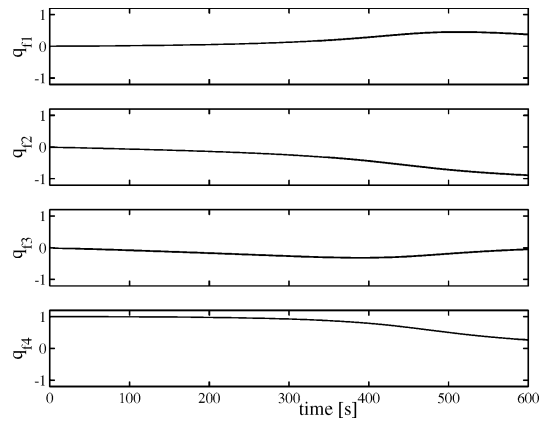where 1 is the N by N identity matrix, k_{δ} is a positive constant, and

$$Q \in \mathbb{R}^{3 \times 2N} \triangleq [E, D]$$

$$W \in \mathbb{R}^{2N \times 2N} \triangleq \begin{bmatrix} w_{s0}e^{-\mu\sigma}1 & 0 \\ 0 & w_g(1 - e^{-\mu\sigma})1 \end{bmatrix} \tag{44}$$
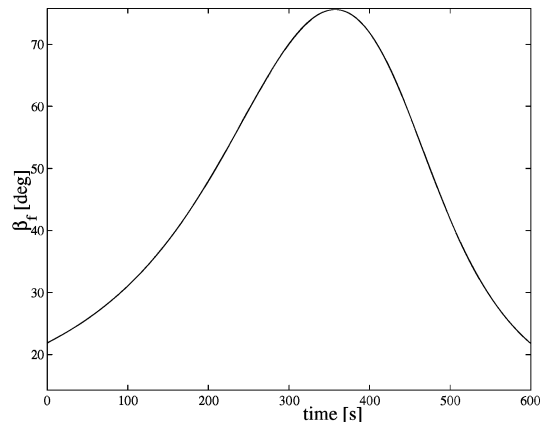
$\sigma \triangleq \det(DD^T)/(I_r^{11}\Omega_0)^2$ being the singularity index, which is zero at the singular sets of gimbal positions. Ω_0 is the nominal spin rate. Moreover w_{s0}, w_g, and μ are positive constants.

a) Ground track of the orbit

b) Reference attitude motion

c) Reference joint motion

Fig. 5 Case 2: reference motion for the tracking control example.

a) Angular velocity errors

b) Attitude errors

c) Joint angle error and torque

d) Actuator spin rates

e) Actuator gimbal rates

f) Actuator gimbal angles

g) Singularity index

h) Required and obtained torque
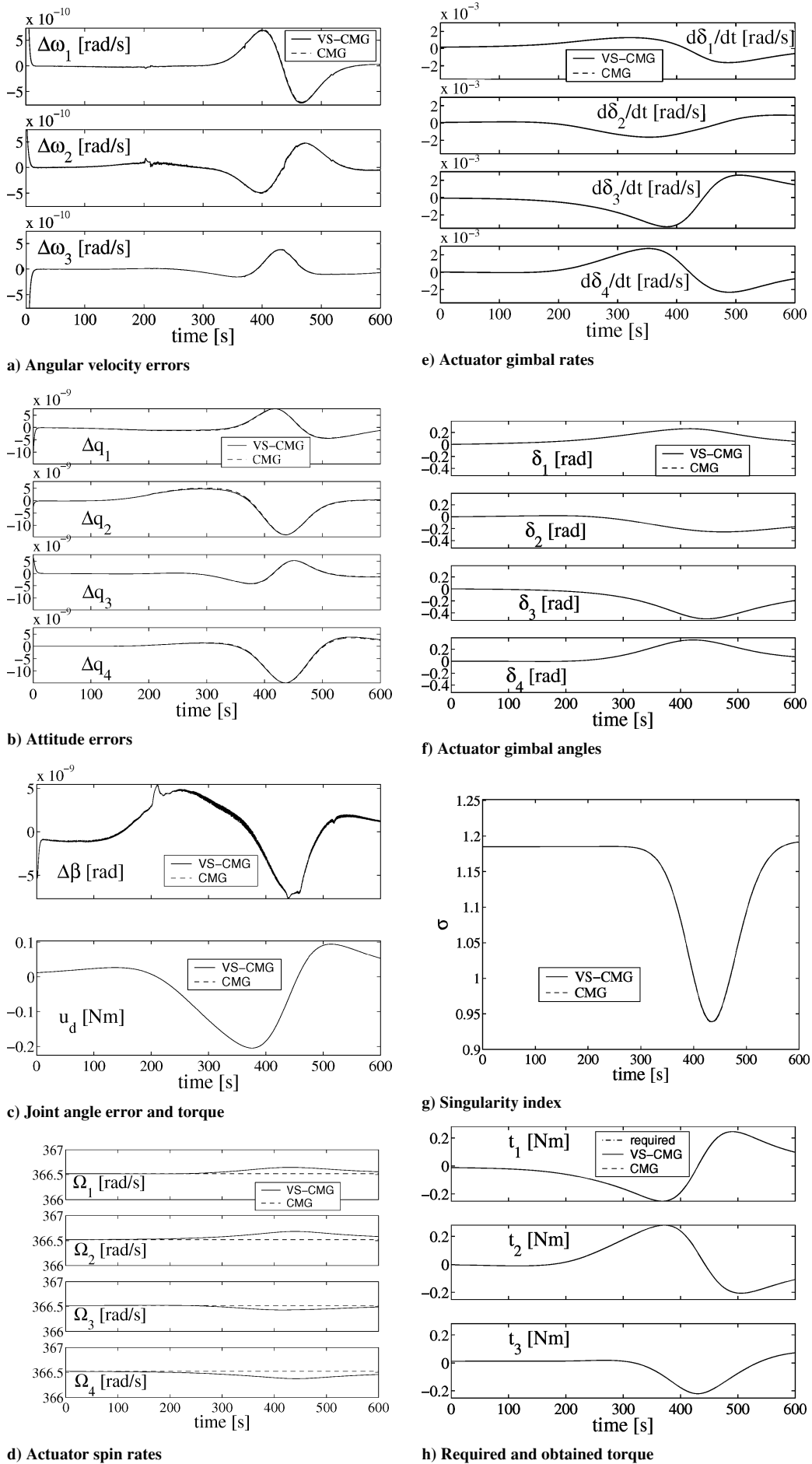
Fig. 6 Results of case 2 (tracking control); use of VS-CMGs compared to use of CMGs.

W is the weight matrix for the pseudoinverse operation in Eq. (43). Far from singularity, the factor $e^{-\mu\sigma}$ is approximately zero, and it approaches one near a singularity. Then, when far from singularity, the required torque is provided by $\ddot{\Delta}$ and $\dot{\Delta}$, and when a singularity is approached, the required torque is provided by $\dot{\Omega}$, which is otherwise close to zero. Therefore, this steering law can effectively overcome the singularity condition and track the required torque. The expression of W in Eq. (44) has been modified with respect to Ref. 7, where the factor of $\mathbf{1}$ in the second law is constant. This produced better performances of the steering law in our simulations.

For the case of simulations with CMGs ($\dot{\Omega} = \mathbf{0}$), we used, instead of Eq. (43), the singularity robust steering law introduced in Ref. 6 and given by

$$\ddot{\Delta} = k_{\dot{\delta}}\mathbf{1}\left[D^T\left(DD^T + \alpha_0 e^{-\mu\sigma}\mathbf{1}\right)^{-1}t_{\mathrm{req}} - \dot{\Delta}\right] \quad (45)$$

where α_0 is a positive constant. This steering law provides singularity robustness by modifying the output torque with respect to the required torque, near singularities. This can have negative effects, as discussed later.

The steering laws in Eqs. (43) and (45) are local singularity avoidance methods, and they can be ineffective on internal elliptic-type singularities.[4] A global avoidance method should be used to guarantee avoidance of singularities in its working domain (as in Ref. 18). However, the use of a global method is considered beyond the scope of the present paper.

V. Simulation Results

The dynamics model, guidance algorithm, control laws and steering laws, which have already been discussed, were coded in MATLAB®–Simulink to conduct the numerical simulations. The simulation code was tested by verification of the conservation of the angular momentum within the numerical accuracy and by repetition of the results of Refs. 6 and 7.

The main objectives of our numerical simulations were 1) to confirm the asymptotic stability of the proposed control law, for regulation and tracking, which has been demonstrated analytically in the preceding section; 2) to study the performances in the ideal case of no external disturbances ($t_e = \mathbf{0}$) and no uncertainties; and 3) to assess the performances preliminarily in case of uncertainties in the knowledge of the system's inertia.

Moreover, the simulations compared the use of VS-CMGs to the use of CMGs and RWs.

As a sample case for our simulations, we considered a dual-body spacecraft, as in Fig. 1b, with mass and geometry data corresponding to the preliminary design of the bifocal relay mirror spacecraft.[11]

We considered a cluster of four VS-CMGs in a pyramid configuration mounted on the transmitter-telescope side of the spacecraft. See Fig. 2, where the vectrix $\mathbb{F}_w$ is parallel to $\mathbb{F}_b$ of Fig. 1b. In this configuration of the VS-CMG cluster, the direction cosines matrix $C_{\mathrm{bg}i}$, defined in Eq. (9), can be conveniently obtained, for each VS-CMG, as the product of three elementary rotations:

$$C_{\mathrm{bg}i} = {}_3C\left(\pi/2\right){}^i{}_1C\left(\pi/2 + \beta_p\right){}_2C\left(\delta_i\right), \qquad i = 1, \ldots, 4 \quad (46)$$

where the notation ${}_jC\left(\eta\right)$ indicates the elementary rotation of the angle η around the jth axis and β_p is the base angle of the cluster pyramid, as in Fig. 2.

The characteristic data of the model used in our simulations are presented in Table 1. In particular, J_c and J_d are the inertia matrices of the transmitter and receiver telescopes (Fig. 1b), and m_c, m_d, r_c, and r_d are as in Eq. (27).

Two sample cases were considered in our simulations: a regulation control case and a tracking control case. For the bifocal relay mirror spacecraft, the regulation case is typical of the attitude slewing to acquire the laser source and the target, and the tracking case is typical of the laser relaying phase. For each of the two control cases, the use of VS-CMGs has been compared with the use of CMGs and RWs. For all of the actuators, the same control law was used, with

a) Angular velocity errors

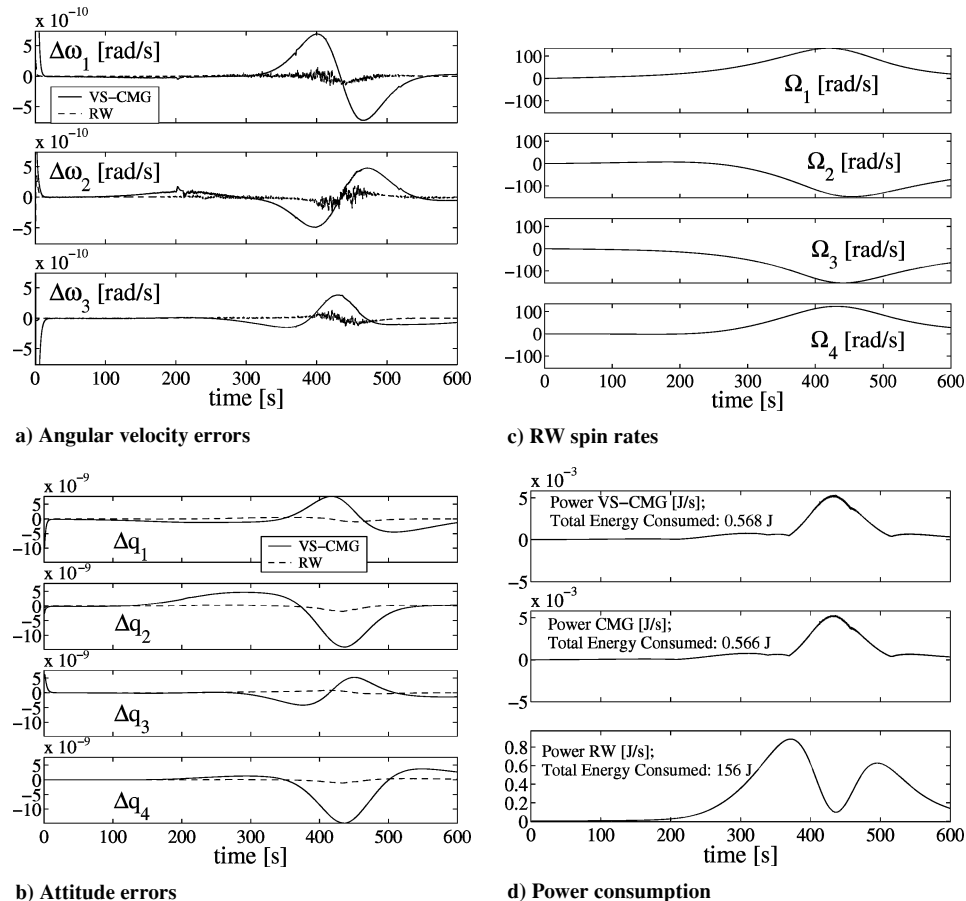b) Attitude errors

c) RW spin rates

d) Power consumption

Fig. 7   Results of case 2 (tracking control); use of VS-CMGs compared to use of RWs.

zeroed $\dot{\Omega}$ in the case of CMGs and zeroed $\dot{\Delta}$ for RWs. In the case of a regulation with RWs, the values of control gains were reduced to avoid quick saturation.

The used control parameters and the saturation values for the actuators are listed in Table 2. Finally, Table 3 gives the values of the initial and target conditions used in the simulations.

The fourth/fifth-order Dormand–Prince algorithm was used for the numerical integrations, with the relative and absolute tolerance set at 10^{-12}.

A. Case 1: Regulation Control (Acquisition Mode)

Figures 3 and 4 report the results of the simulations for the regulation case. In particular, the use of VS-CMGs is compared vs the use of CMGs in Fig. 3 and vs RWs in Fig. 4.

As can be seen in Figs. 3a–3c, the proposed control law is stable and performs satisfactorily well, both with use of the VS-CMGs and the CMGs.

Figure 3g shows that a singularity is encountered after around 5 s of the maneuver. The VS-CMGs perform better than the CMGs in overcoming the singularity. Indeed, the VS-CMGs exploit a variation of the wheel spin rate of about 20 rad/s, as in Fig. 3d. Therefore, the singularity is overcome while the total output torque is maintained near to that required, as shown in Fig. 3h.

Also, the CMGs can overcome the singularity, thanks to the use of the singularity robust steering law, but their output torques significantly fluctuate near the singularity, causing a corresponding fluctuation in the gimbal rates, as can be seen in Fig. 3e. These fluctuations, beyond highly increasing the power consumption, as illustrated in Fig. 4d, are especially critical for flexible spacecrafts and jitter-sensitive payloads.

The RWs are much slower than the VS-CMGs and the CMGs in reaching the commanded attitude, as shown in Figs. 4a and 4b, because of the smaller available torque. Figure 4c reports the wheels' rate variations. The behavior of β is very similar to the case of VS-CMGs and CMGs.

B. Case 2: Tracking Control (Relay Mode)

In this case, simulations are conducted for a sample relay mission of the bifocal relay mirror spacecraft when laser connectivity is

a) Spacecraft angular velocity (regulation)

b) Angular velocity errors (tracking)

c) Spacecraft attitude (regulation)

d) Attitude errors (tracking)

e) Joint angle errors and torque (regulation)

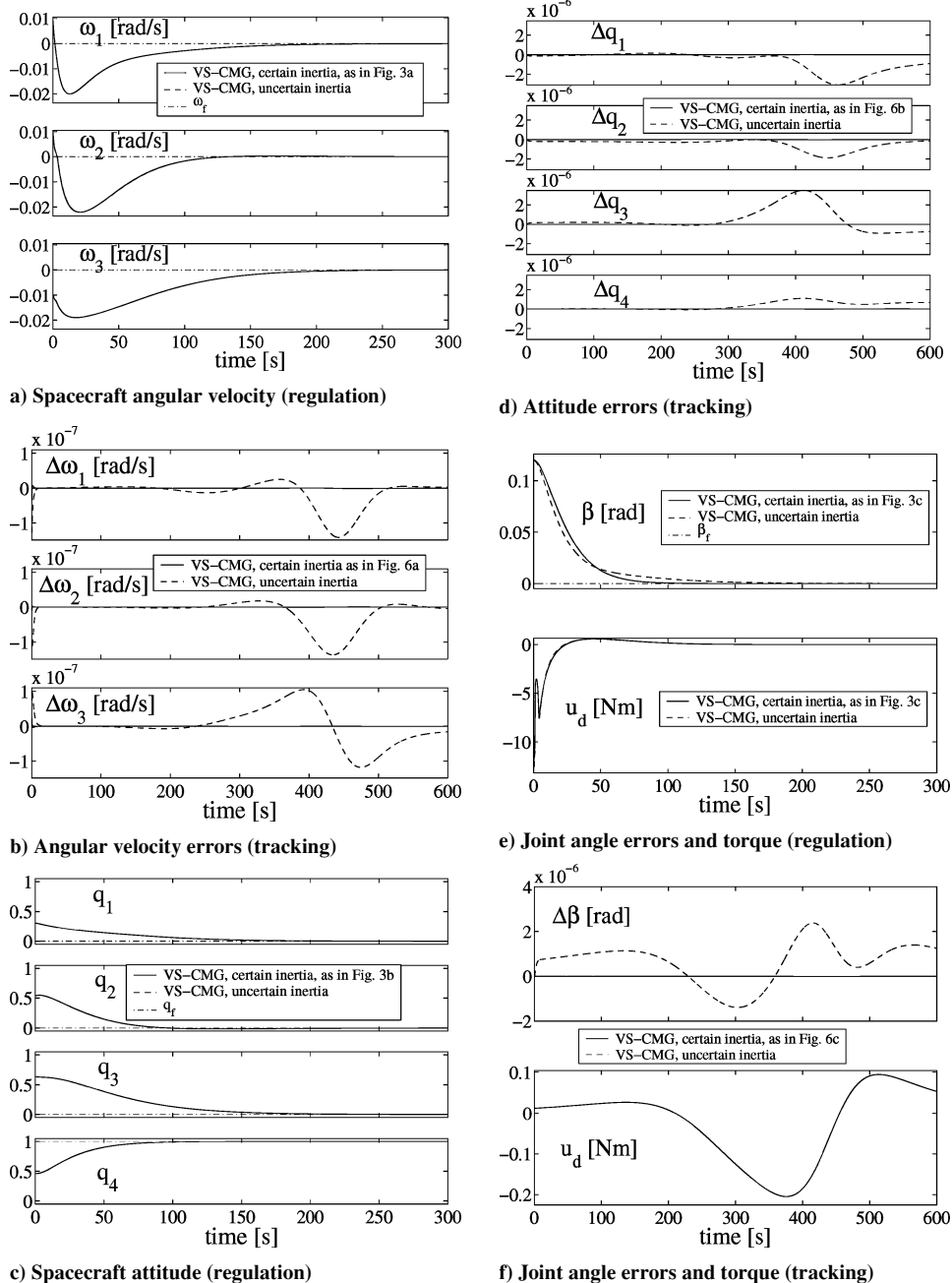f) Joint angle errors and torque (tracking)

Fig. 8   Results of simulations with uncertain inertia matrices: a), c), and e), regulation case; b), d), and f), tracking case.

established between the laser source and the target. In particular, the simulation is started at the precise instant when both the target and the source become visible to the spacecraft.

We considered the target located in Albuquerque, New Mexico, [$-106°-37'$ longitude, $35°3'$ latitude], and the source located in Monterey, California, [$-121°-54'$ longitude, $36°36'$ latitude]. In particular, we considered an orbit passing over the target; indeed, this is one of the dimensioning cases because it requires a high pitch rate. The orbit is circular with an altitude of 715 km. Figure 5a gives the ground track of the orbit. The full line portion indicates the relay phase between the laser source S and the target T. Figures 5b and 5c report the reference attitude and joint-angle motion. The pitch–roll–yaw basis vectors, at the initial condition of the relay maneuver, have been used as basis vectors of the inertial reference frame.

Figure 6 shows the results for the use of VS-CMGs in comparison to CMGs, and Fig. 7 shows the results in case of RWs. In particular, Figs. 6a–6c, 7a, and 7b report the tracking errors.

A singular configuration is approached, but not reached, at around 420 s, as shown in Fig. 6g. A small variation of spin rates is required in the case of VS-CMGs, as reported in Fig. 6d. In this case, both the VS-CMGs and the CMGs provide a torque very near to what is required, as shown in Fig. 6h.

Also, the RWs perform well in this case. The main advantage of the use of the VS-CMGs or the CMGs vs the RWs would be in the considerably smaller energy consumption, as shown in Fig. 7d.

Note that, in the case of VS-CMGs and CMGs, the capability of good performance near singularities depends on the value of the spin angular momentum of the actuators. If the value of nominal angular momentum is reduced, with respect to the aforementioned cases, the advantage of the use of VS-CMGs vs CMGs becomes even more evident.

The designed control law does not guarantee any robustness in the presence of parameter uncertainties or unmodeled dynamics related, for example, to structural flexibility. To assess the performance of the controller in the presence of inertia uncertainties, preliminary simulations were executed for the regulation and tracking cases with VS-CMGs. The estimated inertia matrices used in the control law and steering law for these simulations are as follows:

$$\hat{J}'_{tot} = \begin{pmatrix} 2942 & -664 & 298 \\ -664 & 3903 & 330 \\ 298 & 330 & 5727 \end{pmatrix}, \qquad \hat{J}_d = \begin{pmatrix} 200 & 64 & 179 \\ 64 & 1766 & 73 \\ 179 & 73 & 1648 \end{pmatrix}$$

$$\hat{J}_{(r+g)} = \begin{pmatrix} 0.278 & 0.007 & 0.0024 \\ 0.007 & 0.1469 & 0.0052 \\ 0.0024 & 0.0052 & 0.138 \end{pmatrix}$$

$$\hat{J}_r = \begin{pmatrix} 0.2467 & 0.006 & 0.0002 \\ 0.006 & 0.112 & 0.0044 \\ 0.0002 & 0.0044 & 0.103 \end{pmatrix} \qquad (47)$$

where $\hat{J}'_{tot}$ includes the estimation of the first three terms on the right-hand side of Eq. (27). These inertia values correspond to a relative parameter error of 10%, for the $\hat{J}'_{tot}$ and $\hat{J}_d$, and of 5%, for $\hat{J}_{(r+g)}$ and $\hat{J}_r$, with respect to the values computed with the data in Table 1, which are still used for the truth model of the system dynamics. [Given a parameter vector θ and its estimation $\hat{\theta}$, the relative parameter error is defined in Ref. 19 as $100 \cdot (\| \theta - \hat{\theta} \| / \| \theta \|)$.] Figure 8 gives the results of these two simulations. Despite the uncertainties, the controller still guarantees the stability, as shown in the results of the regulation case reported in Figs. 8a, 8c, and 8e. However, as possibly expected, the parameter uncertainty negatively affects the tracking performances, as shown in Figs. 8b, 8d, and 8f.

VI. Conclusions

The dynamics equations of the motion have been written for a spacecraft model consisting of two rigid bodies connected by a rotational joint: One of the bodies contains a generic number of variable-speed CMGs in a generic cluster configuration. All of the inertia terms have been taken in account.

A guidance algorithm has been developed by consideration of the two bodies of the spacecraft as being optically coupled telescopes and the imposition of the optical connectivity, through the spacecraft, between two distant points on Earth.

A new nonlinear control law, based on Lyapunov's direct method, has been introduced to command the spacecraft attitude and joint displacement. A modified version of an existing acceleration-based steering law has been used.

The results obtained in the simulations with four actuators in a pyramid configuration show that the feedback law performs well, in both the regulation and the tracking control. VS-CMGs perform better than CMGs near singularity configurations. In fact, the output torques of CMGs fluctuate near a singularity, as an effect of the singularity robust steering law, causing a corresponding fluctuation in the gimbal rates. These fluctuations would be critical for flexible spacecraft and jitter-sensitive payloads. In the case of regulation control, the VS-CMGs and CMGs outperform the RWs, as expected. On the contrary, with regard to tracking control, with small initial errors, the performance of all three kinds of actuators are comparable, except that the RWs consume greater energy.

The proposed control law is robust against uncertainties in the knowledge of the inertia terms, as our simulations preliminarily assessed.

References

[1]Girouart, B., Sebbag, I., and Lachiver, J., "Performances of the Pleiades–HR Agile Attitude Control System," *Proceedings of ESA International Conference on Spacecraft Guidance, Navigation and Control Systems*, ESA, Noordwijk, The Netherlands, 2002, pp. 497–500.

[2]Lappas, V., and Steyn, W., "Practical Results on the Development of a Control Moment Gyro Based Attitude Control System for Agile Small Satellites," *Proceedings of AIAA–USU Conference on Small Satellites*, Utah State University, Logan, UT, 2002.

[3]Margulies, G., and Aubrun, J., "Geometric Theory of Single-Gimbal Control Moment Gyro Systems," *Journal of the Astronautical Sciences*, Vol. 26, No. 2, 1978, pp. 159–191.

[4]Bedrossian, N., Paradiso, J., Bergmann, E., and Rowell, D., "Redundant Single-Gimbal Moment Gyroscope Singularity Analysis," *Journal of Guidance, Control, and Dynamics*, Vol. 13, No. 6, 1990, pp. 1096–1101.

[5]Dominguez, J., and Wie, B., "Computation and Visualization of Control Moment Gyroscope Singularities," AIAA Paper 2002-4570, 2002.

[6]Oh, H., and Vadali, S., "Feedback Control and Steering Laws for Spacecraft Using Single Gimbal Control Moment Gyros," *Journal of the Astronautical Sciences*, Vol. 39, No. 2, 1991, pp. 183–203.

[7]Schaub, H., Vadali, S., and Junkins, J., "Feedback Control Law for Variable Speed Control Moment Gyros," *AAS Advances in the Astronautical Sciences: Spaceflight Mechanics*, Univelt, San Diego, 1998, pp. 581–600.

[8]Ford, K., and Hall, C., "Flexible Spacecraft Reorientations Using Gimbaled Momentum Wheels," *Journal of the Astronautical Sciences*, Vol. 49, No. 3, 2001, pp. 421–441.

[9]Yoon, H., and Tsiotras, P., "Spacecraft Adaptive Attitude and Power Tracking with Variable Speed Control Moment Gyroscopes," *Journal of Guidance, Control, and Dynamics*, Vol. 25, No. 6, 2002, pp. 1081–1090.

[10]Agrawal, B. N., and Senenko, C., "Attitude Dynamics and Control of Bifocal Relay Mirror Spacecraft," *AAS Advances in the Astronautical Sciences: Astrodynamics*, Vol. 109, Pt. 3, Univelt, San Diego, 2001, pp. 1703–1720.

[11]Romano, M., and Agrawal, B. N., "Tracking and Pointing of Target by a Bifocal Relay Mirror Spacecraft, Using Attitude Control and Fast Steering Mirrors Tilting," *Proceedings of the AIAA Guidance, Navigation and Control Conference*, AIAA, Reston, VA, 2002.

[12]Romano, M., and Agrawal, B. N., "Acquisition, Tracking and Pointing Control of the Bifocal Relay Mirror Spacecraft," *Acta Astronautica*, Vol. 53, No. 4, 2003, pp. 509–519.

[13]Agrawal, B. N., Romano, M., and Martinez, T., "Three-Axis Attitude Control Simulators for Bifocal Relay Mirror Spacecraft," *AAS Advances in the Astronautical Sciences: Astrodynamics*, Vol. 115, Univelt, San Diego, 2003, pp. 179–192.

[14]Hughes, P. C., *Spacecraft Attitude Dynamics*, Wiley, New York, 1986.

[15]Wertz, J., and Larson, W. J. (eds.), *Space Mission Analysis and Design*, Space Technology Library, Kluwer, Dordrecht, The Netherlands, 1999.

[16]Slotine, J., and Li, W., *Applied Nonlinear Control*, Prentice–Hall, Englewood Cliffs, NJ, 1991.

[17]Junkins, J., and Kim, Y., *Introduction to Dynamics and Control of Flexible Structures*, AIAA Education Series, AIAA, Washington, DC, 1993.

[18]Kurokawa, H., "Constrained Steering Law of Pyramid-Type Control Moment Gyros and Ground Tests," *Journal of Guidance, Control, and Dynamics*, Vol. 20, No. 3, 1997, pp. 445–449.

[19]Tanygin, S., and Williams, T., "Mass Property Estimation Using Coasting Maneuvers," *Journal of Guidance, Control and Dynamics*, Vol. 20, No. 4, 1997, pp. 625–632.